A novel magnesium hydroxide sulfate hydrate whisker-reinforced magnesium silicate hydrate composites

Tingting Zhang[1], Tong Li[1], Ziyu Zhou[1], Min Li[1], Yuan Jia[2,*] and Christopher Cheeseman[3]

[1] Faculty of Infrastructure Engineering, Dalian University of Technology, Dalian 116023, China

[2] Hebei Provincial Key Laboratory of Inorganic Nonmetallic Materials and Hebei Provincial Industrial Solid Waste Comprehensive Utilization Technology Innovation Center, College of Materials Science and Engineering, North China University of Science and Technology, Tangshan 063210, China

[3] Department of Civil and Environmental Engineering, Imperial College London, London SW7 2AZ, United Kingdom

* Correspondence: jia132012@ncst.edu.cn; Tel.: +86-0315-8805020

Abstract

Magnesium hydroxide sulfate hydrate (MHSH) whiskers are used to reinforce magnesium silicate hydrate (M-S-H) cement mortars as novel microfibrous materials because of their similar pH. The microstructure, mechanical performance, and reinforcement mechanism were investigated, and the results showed that the addition of between 1 and 5 wt.% MHSH whiskers improved the compressive and flexural strengths of M-S-H cement mortars. The optimal compressive and flexural strengths were obtained at MHSH whisker contents between 3 and 4 wt.%. The MHSH whiskers had a limited effect on the toughness of M-S-H cement, and mortars reinforced with MHSH whiskers exhibited brittle failure due to the small size of MHSH whiskers and low fiber bridging traction. Scanning electron microscopy (SEM) revealed that the microscale reinforcement mechanism of MHSH whiskers involved whisker pullout, crack deflection, whisker-cement coalition pullout, and whisker fracture. These mechanisms helped dissipate energy and optimize the stress distribution and transfer, which were crucial to improving the flexural strength. The SEM images revealed the rough and grooved surfaces of MHSH whiskers, and X-ray photoelectron spectroscopy (XPS) showed the presence of polar functional groups on the surface which resulted in the adhesion of M-S-H gel on MHSH whiskers due to good interfacial bonding. The mercury intrusion porosimetry (MIP) results indicated that the addition of MHSH whiskers reduced the porosity of M-S-H cement mortars, which also contributed to the increased compressive strength.

Keywords: magnesium silicate hydrate cement; magnesium hydroxide sulfate hydrate whiskers; composite; reinforcement mechanism

1. Introduction

Magnesium silicate hydrate (M-S-H) cementitious material is made by mixing lightly-burned magnesium oxide (MgO) and silica fume (SF) with water, which is of interest recently as it may serve as sustainable alternative to Portland cement. M-S-H cement has a low sintering temperature, which requires less energy consumption and can reduce greenhouse gas emissions. In addition, the low density, low alkalinity, porous structure, and large specific surface area (about 200 m^2/g^{-1}) of this cementitious material can be used to adsorb heavy metal ions and solidify radioactive waste. Alecandre-Franco *et al.* [1] and Sevim *et al.* [2] used magnesium silicate minerals (sepiolite and attapulgite) to adsorb heavy metal ions and toxic organic compounds in wastewater. Fouad *et al.* [3] and Huang *et al.* [4] found that M-S-H gel could adsorb methylene blue (MB), and its adsorption capacity increased upon increasing the surface charge of the M-S-H gel. Zhang *et al.* [5-7] investigated the pH of an M-S-H system and found that its low pH helped solidify aluminum-containing radioactive waste. The latest research has also shown that using M-S-H cement to solidify the radionuclide cesium (Cs) is very effective, and Cs^+ has little effect on the reactions of the M-S-H system [8]. Researchers have also shown that the hydration products of M-S-H cement can form enstatite and forsterite after calcining [9,10], making M-S-H cement an ideal cementitious material for light inorganic fire-proof material.

Despite these applications, research has shown that M-S-H cement is vulnerable to shrinkage deformation, which degrades its mechanical properties. The shrinkage deformation of ordinary concrete mainly occurs via dry shrinkage, which can occur through four main mechanisms: capillary tension, disjoining pressure, surface tension, and interlayer water fluxion [11,12]. Capillary tension mainly results in the dry shrinkage of ordinary Portland cement [13]. Lothenbach *et al.* [14] showed that C-S-H and M-S-H gels are weakly crystalline with unstable chemical compositions. In addition, SiO_2 in C-S-H gels has a chain structure, while it has a layered structure in M-S-H gels. Zhang *et al.* [15] used dilatometry to investigate the shrinkage deformation of M-S-H cement with different sand ratios and proposed a stacked geometry model to explain the observed dry shrinkage.

The strength and toughness of Portland cement mortars can be greatly improved by introducing macro-sized fibers (e.g., steel, glass, and basalt fibers) [16,17] or microfibers (e.g., multiwall carbon nanotubes, silicon carbide whiskers, magnesium borate whiskers, and calcium carbonate whiskers) [18-20]. In particular, whiskers can strengthen, toughen, and reduce the porosity of Portland cement mortars. The introduction of fibers, especially whiskers, is therefore expected to significantly improve the mechanical performances of M-S-H cements. However, no studies of whisker-reinforced M-S-H cement-based pastes have been reported, and the effects of whisker fiber addition on the properties and microstructures of M-S-H cement are currently unknown.

In this study, $MgSO_4 \cdot 5Mg(OH)_2 \cdot 2H_2O$ (MHSH) whiskers, a novel microfibrous material, were used to improve the mechanical properties of M-S-H cement mortars. MHSH whiskers are inorganic single crystals with a pH of 9-9.5 [21], which is similar to the pH of M-S-H cement, suggesting that MHSH whiskers will have a good compatibility with M-S-H cement. This study aimed to improve the shrinkage and investigate and enhance the mechanical properties and toughness of MHSH whisker-reinforced M-S-H cement composites. The microstructure (e.g., morphology and interfacial bonding between M-S-H gels and MHSH whiskers) at different reaction stages was also analyzed to understand the reinforcement mechanism to provide a theoretical basis for further applications.

2. Materials and methods

2.1 Materials

M-S-H cement mortars were prepared using MgO (MagChem 30, MAF Magnesite B.V., The Netherlands), silica fume (SF, 920U, Elkem Materials Ltd., China), standard silica sand with particle sizes in the range from 0.21 mm to 0.36 mm (Xinlian Silica Sand, Zhuanghe, China), and sodium hexametaphosphate ($(NaPO_3)_6$, Na-HMP, China National Pharmaceutical Group Corporation, China). The chemical compositions of these materials and MHSH whiskers are given in Table 1.

MHSH whiskers were 10 - 60 μm long with diameters of <1.0 μm and were purchased from Kaishefeng Industrial Co., Ltd., Shanghai, China. A SEM image and the XRD pattern of the MHSH whiskers are shown in Fig. 1 and Fig. 2, respectively.

2.2 Methods

2.2.1 Sample preparation

The ratios of raw materials used to prepare the M-S-H mortar samples are shown in Table 2. Fiber-reinforced samples were prepared with 1 to 5 wt.% MHSH whiskers relative to the M-S-H cement binder. 2 wt.% of Na-HMP relative to the solids in the M-S-H cement was initially dissolved in the mix water. MgO, MHSH whiskers, and silica fume (SF) were then slowly added into the Na-HMP solution with continuous stirring. Silica sand was finally added using a rotary mixer to obtain the M-S-H mortars which were then pressed into steel molds to obtain 40 mm × 40 mm × 160 mm prisms and 40 mm × 40 mm × 40 mm cubic samples. The molds were vibrated for 3 min to minimize voids in the samples which were then cured at 95% relative humidity and 20 ℃. After 24 h, the samples were de-molded and stored at 95% relative humidity for 7, 14, and 28 days prior to testing.

2.2.2 Mechanical performance testing

The 40 mm × 40 mm × 160 mm and 40 mm × 40 mm × 40 mm samples were used to determine the flexural and compressive strengths using a computer-controlled electro-hydraulic servo universal tester (WHY-300/10, Hualong Testing Instrument Co., Ltd., Shanghai, China, Chinese Standard GB/T 17671-1999). The compressive strengths of samples were determined at a loading rate of 2400 ± 200 N/s, while the 40 mm × 40 mm × 160 mm samples were subjected to 3-point bending tests using a 100 mm span at a loading rate of 50 ± 10 N/s. Three samples were tested during each test and for each composition and curing time.

2.2.3 Characterization

Samples were dried in a vacuum oven, ground into powder, and then passed through a 0.075 mm sieve. X-ray diffraction (XRD, D8 Advance with Cu Kα, Bruker, Karlsruhe, Germany) was used to identify the crystalline phases present in the samples ($2\theta = 5°-80°$). X-ray photoelectron spectrometry (XPS, Monochromatic Al Kα 1486.6 eV X-ray source, ESCALAB XI+, Thermo, England) was used to identify the chemical bonds and functional groups present in the MHSH whiskers. X-ray fluorescence spectrometry (XRF, SRS4300, Bruker, Karlsruhe, Germany) was used to determine the chemical composition of the raw materials.

Fourier-transform infrared spectroscopy (FTIR, EQUINOX55, Bruker, Karlsruhe, Germany) was used to determine the chemical bonds and functional groups present in the hydration products. Hydrated samples were mixed with potassium bromide powder in a ratio of 1:100, and the mixtures were pressed into 0.5 mm thick disc samples with 13 mm diameters.

Scanning electron microscopy (SEM, Nova NanoSEM-50, FEI Company, Hillsboro, OR, USA) was used to study the microstructure of the hydrated products. Samples were gold-coated prior to SEM analysis.

Mercury intrusion porosimetry (MIP, AutoPore IV9500, McMurray Instruments, Atlanta, GA, USA) was used to characterize the pore structures of the M-S-H cement samples. Samples were dried by soaking in ethanol for 24 hours and allowing the ethanol to fully evaporate. The samples were then dried in a vacuum oven at 60 ℃ for 48 h and inserted into a dilatometer glass measuring tube for MIP.

3. Results and discussion

3.1 Mechanical properties testing

The compressive and flexural strengths of M-S-H mortars are shown in Fig. 3 and 4. The flexural strengths of composites containing MHSH whiskers were higher than those of the control samples. Samples containing 4 wt.% MHSH whiskers exhibited the highest flexural strengths of 4.2 MPa and 6.0 MPa after 14 d and 28 d, respectively. The composite sample containing 3 wt% MHSH whisker had the highest compressive strength (60.1 MPa after 28 d).

MHSH whiskers and M-S-H cement formed strong interfacial bonds, and as the applied load increased, whisker pullout, crack deflection, and whisker breakage occurred, reducing the stress concentration at crack tips and increasing the compressive and flexural strengths of the composites. When the curing time was less than 7d, the role of MHSH whiskers to improve the compressive and flexural strengths of the composites is less obvious. As the curing time increased, the role of MHSH whiskers to improve the compressive and flexural strengths of the composites increased. The compressive and flexural strengths of the composites increased and then decreased as the MHSH whisker content increased. After 28 d, the flexural strength of samples with 4 wt.% whiskers increased by 17.6%, while the compressive strength of the sample with 3 wt.% whiskers increased by 13.1%. The mechanical properties of the M-S-H mortar increased due to the increased bonding between the MHSH whiskers and M-S-H cement during curing. The reinforcement of MHSH whiskers increased, improving the mechanical performance of the M-S-H cement. In addition, whisker agglomeration may have occurred at higher whisker contents, which reduced the mechanical performance of the M-S-H cement.

The load-deflection curves of the M-S-H cement mortars are shown in Fig. 5. These are similar, but their slopes decreased as the MHSH whisker content increased, indicating a positive correlation between the toughness of the M-S-H cement mortar and the MHSH whiskers content. However, the addition of MHSH whiskers did not change the brittleness of the M-S-H cement mortar. Table 3 shows that as the content of MHSH whiskers increased from 1 to 5%, the peak load of the M-S-H cement mortar increased by 20.1%.

3.2 Characterization

In order to investigate the reinforcing mechanism of MHSH whiskers and to clarify the chemical composition and morphology of M-S-H cement mortars, samples were characterized by XRD, XPS, and SEM.

3.2.1 Phase analysis

Fig. 6 shows the XRD patterns of M-S-H cement mortars containing 0 to 5 wt.% MHSH whiskers after curing for 28 d. Diffraction peaks were observed at 2θ values of 12.9 °, 17.2 °, and 22.7 ° [22], and peak intensities increased with the MHSH whiskers content. The intensity of the peak corresponding to $Mg(OH)_2$ increased with MHSH whiskers content because MHSH whiskers contain $Mg(OH)_2$.

XRD patterns of samples with 5 wt% MHSH whiskers after different curing periods are shown in Fig. 7. After curing for 1 d the diffraction peak corresponding to $Mg(OH)_2$ was attributed to $Mg(OH)_2$ in the whiskers. As curing proceeded, the intensity of the $Mg(OH)_2$ diffraction peak increased, while the diffraction peaks corresponding to MgO decreased. After 7 d of curing M-S-H gel was detected (2θ = 35.0 ° and 60.0 °) [23]. The decrease in the intensities of the MgO and $Mg(OH)_2$ peaks at 43.0 ° and 62.0 ° with curing time indicated that brucite continued to react with SF, and new diffraction peaks were not observed. It was concluded that the enhanced mechanical properties of the MHSH whisker-reinforced M-S-H cement mortars were attributed to the interfacial bonding between MHSH whiskers and the M-S-H cement matrix. The decreased porosity was also due to the inclusion of MHSH whiskers.

3.2.2 Chemical composition and morphology

Interfacial bonding plays a key role in the strengthening, toughening, and crack resistance of fiber-reinforced cement-based composites [24]. The microscale reinforcement mechanism of MHSH whiskers involves whisker pullout, crack deflection, whisker-cement coalition pullout, and whisker fracture, as shown in Figs. 8 and 9. The M-S-H gel and whisker surfaces formed strong interfacial bonds which played a dominant role in strengthening the MHSH whisker-reinforced M-S-H cement composites. The adhesion of M-S-H gel to the whisker surface can be divided into three stages. In the first stage (early stage of hydration), SF spheres contacted the MHSH whiskers to allow the growth of M-S-H gels. This was confirmed by the EDS patterns of the target area in Fig. 8a, which shows that the atomic contents of Si and S were 13.27% and 0.78%, respectively. During the second stage, $Mg(OH)_2$ reacted with silica fume, and M-S-H gel appeared on the surface as curing proceeded. The M-S-H gel expanded, and the MHSH whiskers were coated with M-S-H gel, as shown in Fig. 8b. The atomic content of Si increased to 13.3%, while that of S decreased to 0.45%, indicating that the M-S-H layer attached to the whisker surface gradually thickened, causing the bonding strength of the MHSH whiskers and M-S-H cement to continuously increase. The bonding strength between the MHSH whiskers and M-S-H cement increased with the curing time. In the third stage (late stage of hydration), the M-S-H gel was completely attached to the MHSH whiskers, as shown in Fig. 8c. The atomic content of Si increased to 15.6%, while that of S decreased to 0.4%, indicating that the M-S-H gel layer increased, and the bonding strength further increased. This was responsible for the improved strength and toughness of M-S-H cement mortars containing MHSH whiskers.

Whisker pullout and fracture also have an important effect on reinforcement, as confirmed by EDS analysis of the target area (Fig. 9a). The whisker surfaces contain S, O, and Si, indicating that the whiskers and cement formed strong interfacial bonds that improved the mechanical performance of the M-S-H cement. As the external stress increased, the MHSH whiskers and the M-S-H cement matrix detached from each other, as shown in Fig. 9b-10a. The M-S-H matrix doesn't contain S, but the S presents in the holes indicated the whisker surface is stripped due to the strong bonding between the MHSH whisker and M-S-H cement in the process of whisker pulling out, so that some MHSH whiskers are left in the holes. Energy was dissipated via friction between whiskers and the cement matrix during whisker pull-out, and the initiation and rapid propagation of fractures were hindered which increased the tensile strength of the composite [25-27].

As the external stress increased, cracks were initiated in the cement matrix but were terminated when they reached the whiskers [28]. However, the stress concentration created by the crack may have caused whisker fracture and crack propagation. In this scenario, energy dissipation was still achieved, although whisker breakage occurred via brittle fracture, causing the peak load to increase [29,30]. This may explain the increased peak load of mortars containing MHSH whiskers (Fig. 10b). The energy dissipation by MHSH whiskers during the two toughening mechanisms effectively reduced the stress concentration at the crack tips and optimized the stress distribution and transfer, thus improving the compressive strength, flexural strength, and other properties of the composite.

Interfaces play an important role in the mechanical performance of cement-based composites [31]. The adhesion of M-S-H gel to whisker surfaces formed strong interfacial bonds, as shown in Fig. 9. The surfaces of MHSH whiskers were rough, and grooves expanded outwards along the whiskers, increasing their specific surface area. Because of this, the whiskers preferred to become mechanically embedded with SF spheres and were closely combined, which was beneficial to the adhesion of M-S-H gels on whiskers. Therefore, the rough and grooved surfaces of the MHSH whiskers were secondary cause of the adhesive growth of M-S-H gel on whiskers. The XPS spectrum of MHSH whiskers in Fig. 11 shows that the interfacial components mainly consisted of C, O, S, and Mg, with binding energies of 285 eV, 532 eV, 171 eV, and 1303 eV, respectively.

The spectra indicate the presence of a large amount of O and a small proportion of S. XPS Peak software was used for peak splitting of the O 1s narrow spectrum. Fig. 12 shows the fitted O 1s spectra, which contained two peaks with binding energies of 531.8 eV and 533.7 eV, which corresponded to -OH and S=O, respectively. Wei *et al.* [9] claimed that silicic acid precipitates were generated on wetted surfaces of SF spheres, via the reaction shown in Eq. 1. Fig. 12 indicates that the MHSH whisker surfaces contain many polar functional groups. When the SF spheres came into contact with the MHSH whiskers, the polar functional groups (-OH) on the whisker surfaces bound to the silicic acid precipitates, closely binding the SF spheres and MHSH whiskers. This was the primary cause of the adhesion of the M-S-H gel on the whiskers.

$$SiO_{2(s)} + 2H_2O_{(l)} \rightarrow H_2SiO_{4(surface)} \quad \text{Eq.1}$$

3.3. Porosity analysis

M-S-H cement is a porous material, and pores have significant effects on properties, including drying shrinkage, strength, creep behavior, thermal conductivity, water absorption, permeability, and corrosion resistance. The pore size distribution and cumulative pore volume curves of M-S-H cement with 0-5 wt.% MHSH whiskers are shown in Fig. 13. The addition of MHSH whiskers reduced the porosity of the magnesium silicate cement matrix and eliminated pores with sizes of 5 - 50 nm. When the MHSH whisker content was 3 wt.%, the optimal filling effect was achieved, and whisker agglomeration was observed upon further increasing the MHSH whisker content (> 3 wt.%). The pore density also increased, while the compressive strength of M-S-H cement mortar decreased. The cumulative pore volume of M-S-H cement increased as the pore diameter decreased, as shown in Fig. 13b. When the pore diameter was < 10 nm, the cumulative pore volume significantly increased. The results showed that the pores in the M-S-H cement were mainly gel pores < 10 nm. In addition, the cumulative pore volume of the M-S-H cement paste without whiskers rapidly increased to 10 - 20 nm, while that of the whisker-reinforced M-S-H cement composites slowly increased to 10 - 20 nm. When the MHSH whiskers content was 3%, the optimal effect was achieved, indicating that pores with sizes of 10 - 20 nm were filled.

The pore and pore volume distributions of M-S-H cement with 0-5wt.% MHSH whiskers are shown in Fig. 14. The porosity of the M-S-H cement decreased as the whisker content increased and reached a minimum at an MHSH whisker content of 3 wt.%. Pores with diameters below 10 nm dominated the pore volume distribution, followed by those with diameters of 10 - 50 nm. Mindess *et al.* [32] proposed that pores with diameters of 10 - 100 nm significantly affected the mechanical properties of cement, while the present study suggests that the MHSH whiskers in the M-S-H cement mainly filled pores with diameters < 50 nm and also improved the mechanical properties of the M-S-H cement. For porous materials with a constant matrix strength and pore size distribution, the strength is proportional to the porosity, and the compressive strength of the M-S-H cement increased with the whisker content [33,34]. The pore size distribution also affects the strength of a material [35-38], and MHSH whiskers filled the pores in M-S-H cement, which eliminated pores that adversely affected the mechanical properties and optimized the pore size distribution.

In cement paste strength theory, researchers have established more than 10 semi-empirical equations to describe the relationship between porosity and strength [39,40]. Among them, the most representative and widely used are the Balshin, Ryshkevitch, Schiller, and Hasselmann equations [41]. According to the results of this article, the M-S-H cement porosity-strength model was best described by the Ryshkevitch equation among the Balshin, Ryshkevitch, Schiller, and Hasselmann equations, as shown in Fig. 15. The porosity and compressive strength of M-S-H cements were inversely proportional, and the compressive strength increased as the porosity decreased. When the MHSH whiskers content was less than 3 wt.%, the MHSH whiskers were uniformly dispersed with no obvious aggregation. The porosity had a greater impact on the M-S-H compressive strength compared with the MHSH whiskers. The aggregation of whiskers was observed as the MHSH whisker content further increased (> 3 wt.%), the pore density increased, and the compressive strength of the M-S-H cement mortar decreased. However, the incorporation of MHSH whiskers not only improved the slurry density but also acted as a skeleton support, and the compressive strength increased as the MHSH whiskers content increased. At this point, the MHSH whiskers had a greater impact on the M-S-H compressive strength compared with the porosity.

4. Conclusions

1) The addition of MHSH whiskers improved the compressive and flexural strengths of M-S-H cement mortars. After 28 d curing, the flexural strength of samples with 4 wt.% whiskers increased by 17.6%, and the compressive strength of the sample with 3 wt.% whiskers increased by 13.1%. However, the MHSH whiskers had a negligible effect on the toughness of M-S-H cement mortar, which still displayed brittle fracture, due to the small size of MHSH whiskers and the limited effect of fiber bridging traction.

2) The microscale reinforcement mechanism of MHSH whiskers involves whisker pullout, crack deflection, whisker-cement coalition pullout, and whisker fracture. These mechanisms effectively dissipated energy and optimized the stress distribution and transfer, thus improving the compressive strength, flexural strength, and other properties of the composites.
3) The surfaces of MHSH whiskers were rough, grooved, and coated with polar functional groups. This promoted adhesion between the M-S-H gel and MHSH whiskers and allowing the MHSH whiskers and cement matrix to strongly bond with each other.
4) The MHSH whiskers filled pores, which eliminated pores with adverse effects and optimized the pore size distribution, improving the compressive strength of the M-S-H cement. MHSH whiskers had a good filling effect for 10 - 20 nm pores, with an optimal effect at 3 wt.% whiskers. As the whisker content increased further, whisker agglomeration occurred, and the density of pores increased, which reduced the porosity, resulting in a less-homogeneous pore size distribution, and decreasing the compressive strength of the M-S-H cement.
5) According to the results of this article, the M-S-H cement porosity-strength model was best described by the Ryshkevitch equation. The model indicate that, the porosity and compressive strength of M-S-H cements were inversely proportional, and the main factor that influences mechanical properties of M-S-H cement is porosity and MHSH whiskers dosages.

Acknowledgments

The authors wish to express their gratitude and sincere appreciation for the financial support by the national natural science foundation of China (Grant No. 51778101; No. 51808217), national key R&D program of China (2017YFE0107000), natural science foundation of Hebei province (E2019209403)，the fundamental research funds for the central universities (DUT19JC27), state key laboratory of coastal and offshore engineering of Dalian university of technology (Grant No. LP1808).

References

[1] Maria AF, Angel AL, Vicente GS. An identification study of vermiculites and micas: adsorption of metal ions in aqueous solution. Fuel Process. Technol 2011; 92(2): 200-205.

[2] Sevim AM, Hojiyev R, Gül A, Çelik MS. An investigation of the kinetics and thermodynamics of the adsorption of a cationic cobalt porphyrazine onto sepiolite. Dyes Pigm. 2011; 88(1): 25-38.

[3] Ferrero F. Adsorption of methylene blue on magnesium silicate: kinetics, equilibria and comparison with other adsorbents. J. Environ. Sci 2010; 22(3): 467-473.

[4] Huang R, He L, Zhang T, Li D, Tang P, Zhao Y, Feng Y. Fabrication and adsorption behavior of magnesium silicate hydrate nanoparticles towards methylene blue. Nanomaterials 2018; 8(5): 271.

[5] Zhang TT, Cheeseman CR, Vandeperre LJ. Development of low pH cement systems forming magnesium silicate hydrate (M-S-H). Cement Concr Res 2011; 41: 439-442.

[6] Zhang TT, Vandeperre LJ, Cheeseman CR. Magnesium-silicate-hydrate cements for encapsulating problematic aluminium containing wastes. J.Sustainable Cement-Based Mater. 2012; 1: 34-45.

[7] Zhang TT, Vandeperre LJ, Cheeseman CR. Formation of magnesium silicate hydrate (M-S-H) cement pastes using sodium hexametaphosphate. Cement Concr Res 2014; 65: 8-14.

[8] Zhang TT, Li T, Zou J, Li YM, Zhi SW, Jia Y, Cheeseman. Immobilization of radionuclide Cs by magnesium silicate hydrate cement. Mater. 2019; 13(1): 146.

[9] Li ZH, Zhang TS, Hu J, Tang Y, Niu YF, Wei JX, Yu QJ. Characterization of reaction products and reaction process of MgO-SiO_2-H_2O system at room temperature. Constr Build Mater 2014; 61(7): 252-259.

[10] Jin F, Al-Tabbaa A. Thermogravimetric study on the hydration of reactive magnesia and silica mixture at room temperature. Thermochim. Acta 2013; 566(16): 162-168.

[11] Tennis PD, Jennings HM. A model for two types of calcium silicate hydrate in the microstructure of Portland cement pastes. Cement Concr Res 2000; 30(6): 855-863.

[12] Allen AJ, Jennings HM, Thomas JJ. Composition and density of nanoscale calcium-silicate-hydrate in cement. Nat. Mater. 2007; 6(4): 311-316.

[13] Yan FU, Ping GU, Ping XIE, Beaudoin JJ. Development of eigenstress due to drying shrinkage in hardened Portland cement pastes: thermomechanical analysis. Cement Concr Res 1994; 24(6): 1085-1090.

[14] Lothenbach B, Nied D, L'Hopital E, Achiedo G, Dauzères A. Magnesium and calcium silicate

hydrates. Cement Concr Res 2015; 77: 60-68.

[15] Zhang TT, Liang XM, Li CM, Lorin M, Li Y, Vandeperre LJ, Cheeseman CR. Control of drying shrinkage in magnesium silicate hydrate (M-S-H) gel mortars. Cement Concr Res 2016; 88: 36-42.

[16] Qin J, Qian J, Li Z, You C, Dai X, Yue Y, Fan YR. Mechanical properties of basalt fiber reinforced magnesium phosphate cement composites. Constr Build Mater 2018; 188: 946-955.

[17] Xue GL, Yilmaz E, Song WD, Cao S. Analysis of internal structure behavior of fiber reinforced cement-tailings matrix composites through X-ray computed tomography. Compos Part B 2019; 175: 107091.

[18] Park HM, Park SM, Lee S, Shon I, Jeon H, Yang BJ. Automated generation of carbon nanotube morphology in cement composite via data-driven approaches. Compos Part B 2019; 167: 51-62.

[19] An J, Nam BH, Alharbi Y, Cho BH, Khawaji M. Edge-oxidized graphene oxide (EOGO) in cement composites: cement hydration and microstructure. Compos Part B 2019; 173: 106795.

[20] Tafesse M, Kim HK. The role of carbon nanotube on hydration kinetics and shrinkage of cement composite. Compos Part B 2019; 169: 55-64.

[21] Ma X, Ning G, Qi C, Gao J. One-step synthesis of basic magnesium sulfate whiskers by atmospheric pressure reflux. Particuology 2016; 24: 191-196.

[22] Ding Y, Zhang G, Zhang S, Huang X, Yu W, Qian Y. Preparation and characterization of magnesium hydroxide sulfate hydrate whiskers. Chem Mater 2000; 12: 2845-2852.

[23] Brew DRM, Glasser FP. Synthesis and characterisation of magnesium silicate hydrate gels. Cement Concr Res 2005; 35: 85-98.

[24] Pi ZY, Xiao HG, Liu R, Liu M, Li H. Effects of brass coating and nano-SiO_2 coating on steel fiber−matrix interfacial properties of cement-based composite. Compos Part B 2020; 189: 107904.

[25] Giosuè C, Mobili A, Yu QL, Brouwers HJH, Tittarelli RF. Properties of multifunctional lightweight mortars containing zeolite and natural fibers. J. Sustainable Cement-Based Mater 2019; 8(4): 214-227.

[26] Zheng Y, Zhang P, Cai Y, Jin Z, Moshtagh E. Cracking resistance and mechanical properties of basalt fibers reinforced cement-stabilized macadam. Compos Part B 2019; 165: 312-334.

[27] Ombres L. Concrete confinement with a cement based high strength composite material. Compos Struct 2014; 109: 294-304.

[28] Xue GL, Yilmaz E, Song WD, Cao S. Mechanical, flexural and microstructural properties of

cement-tailings matrix composites: Effects of fiber type and dosage. Compos Part B 2019; 172: 131-142.

[29] Dong SF, Han BG, Yu X, Ou JP. Constitutive model and reinforcing mechanisms of uniaxial compressive property for reactive powder concrete with super-fine stainless wire. Compos Part B 2019; 166: 298-309.

[30] Su ZH, Guo L, Zhang ZH, Duan P. Influence of different fibers on properties of thermal insulation composites based on geopolymer blended with glazed hollow bead. Constr Build Mater 2019; 203: 525-540.

[31] Petrella A, Spasiano D, Liuzzi S, Ayr U, Cosma P, Rizzi V, Mundo RD, Petrella M. Use of cellulose fibers from wheat straw for sustainable cement mortars. J. Sustainable Cement-Based Mater 2019; 8(3): 161-179.

[32] Mindess S, Young JF. Concrete. prentice-hall, Inc: Englewood Cliffs, NJ, 1981.

[33] Shaikh FU, Nishiwaki T, Kwon S. Effect of fly ash on tensile properties of ultra-high performance fiber reinforced cementitious composites (UHP-FRCC). J. Sustainable Cement-Based Mater 2018; 7(6): 357-371.

[34] Bao JW, Xue SB, Zhang P, Dai ZZ, Cui YF. Coupled effects of sustained compressive loading and freeze-thaw cycles on water penetration into concrete. Struct. Concr, 2020; 1-11.

[35] Ahmad M R, Chen B, Yu J. A comprehensive study of basalt fiber reinforced magnesium phosphate cement incorporating ultrafine fly ash. Compos Part B 2019; 168: 204-217.

[36] Zhang ZH, Zhu YC, Zhu HJ, Zhang Y, Provis JL, Wang H. Effect of drying procedures on pore structure and phase evolution of alkali-activated cements. Cement Concr Compos 2019; 96: 194-203.

[37] Xue SB, Zhang P, Bao JW, He LF, Hu Y, Yang SD. Comparison of mercury intrusion porosimetry and multi-scale X-ray CT on characterizing the microstructure of heat-treated cement mortar. Mater. Charact. 2020; 160: 110085.

[38] Wang SF, Ma X, He L, Zhang ZH, Li LF, Li YX. High strength inorganic-organic polymer composites (IOPC) manufactured by mold pressing of geopolymers. Constr Build Mater 2019; 198: 501-511.

[39] Song Q, Zhao HY, Jia JW, Yang L, Lv W, Bao JW, Shu XQ, Gu QX, Zhang P. Pyrolysis of municipal solid waste with iron-based additives: A study on the kinetic, product distribution and

catalytic mechanisms. J Clean Prod 2020; 258: 120682-120696.

[40] Wang YR, Cao Y, Zhang P, Ma Y, Zhao T, Wang H, Zhang Z. Water absorption and chloride diffusivity of concrete under the coupling effect of uniaxial compressive load and freeze-thaw cycles. Constr Build Mater 2019; 209: 566-576.

[41] Bao JW, Li SG, Zhang P, Ding X, Xue S, Cui Y, Zhao T. Influence of the incorporation of recycled coarse aggregate on water absorption and chloride penetration into concrete. Constr Build Mater 2020; 239: 117845.

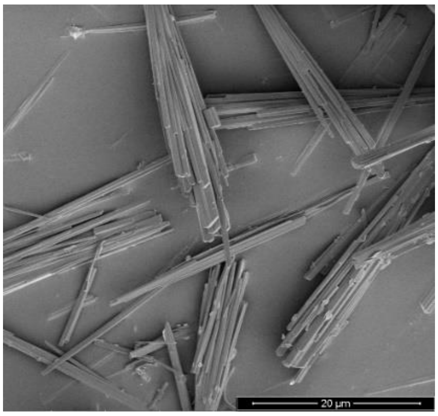

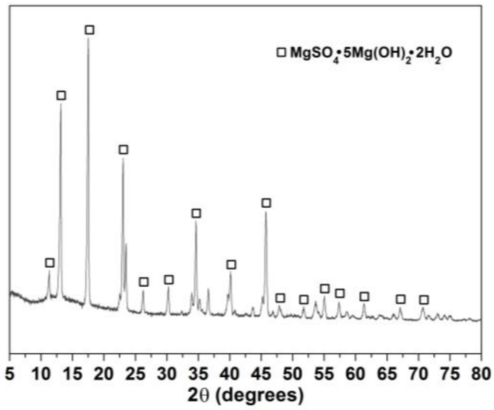

Fig. 1. SEM image of MHSH whiskers.

Fig. 2. XRD pattern of MHSH whiskers.

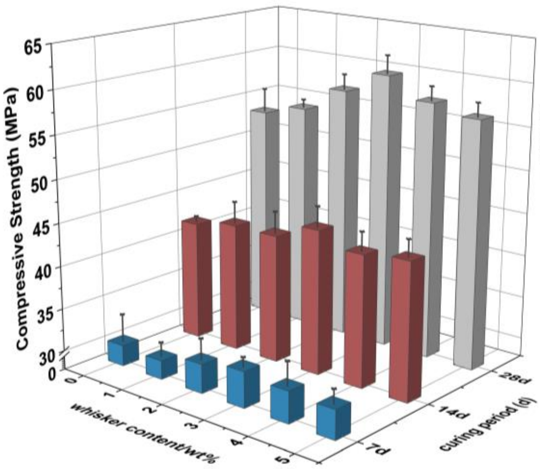

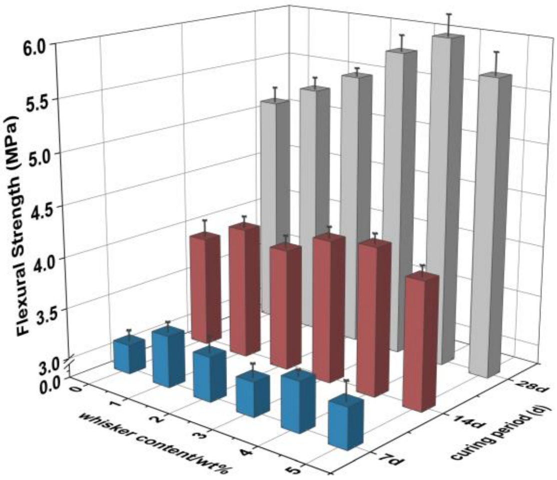

Fig.3. Compressive strength data.

Fig.4. Flexural strength data.

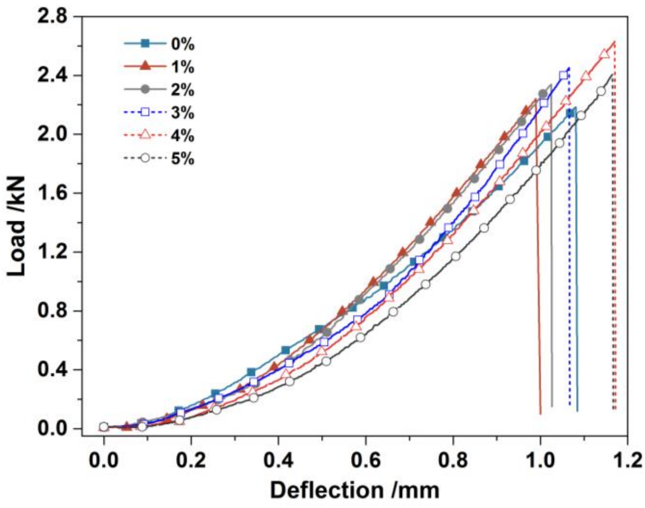

Fig. 5. Flexural load defection curves of different samples after 28 d.

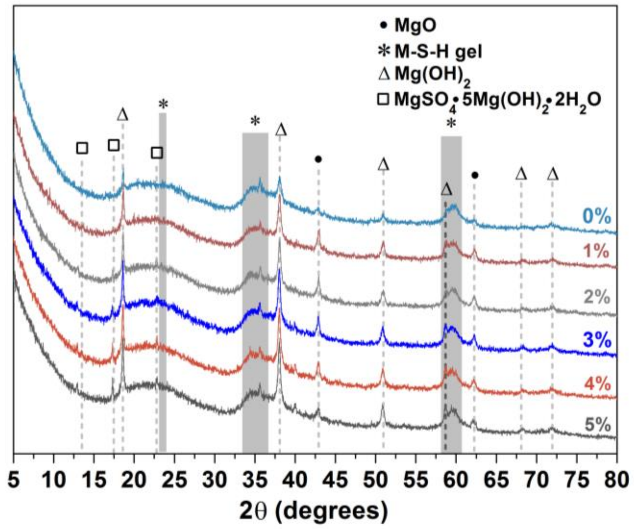

Fig.6. XRD data of M-S-H cement mortars with 0-5 wt% MHSH whiskers cured for 28 d.

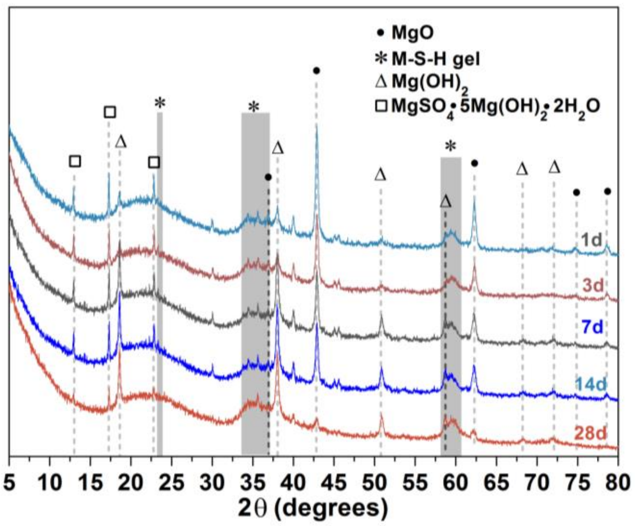

Fig.7. XRD data of M-S-H mortars with 5 wt% MHSH whiskers after different curing times.

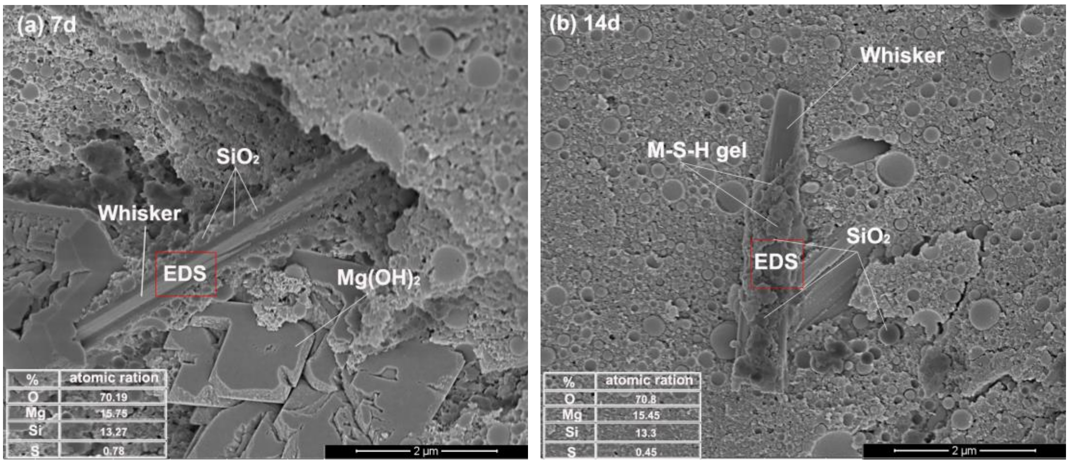

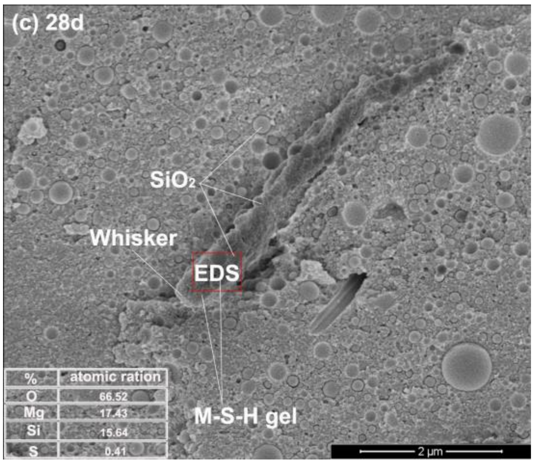

Fig.8. SEM and EDS images of M-S-H with 5 wt% MHSH whiskers after different curing periods.

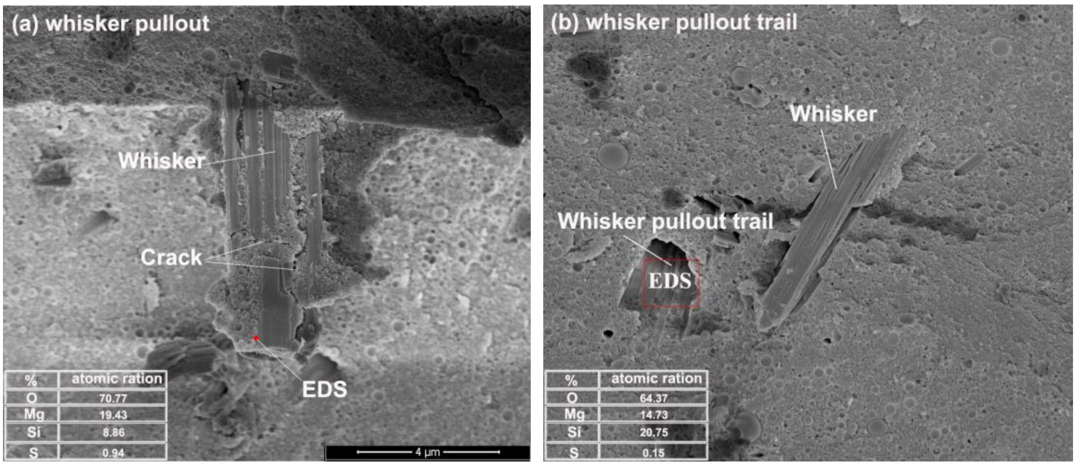

Fig.9. SEM images and EDS analysis of M-S-H with 5 wt% MHSH whiskers.

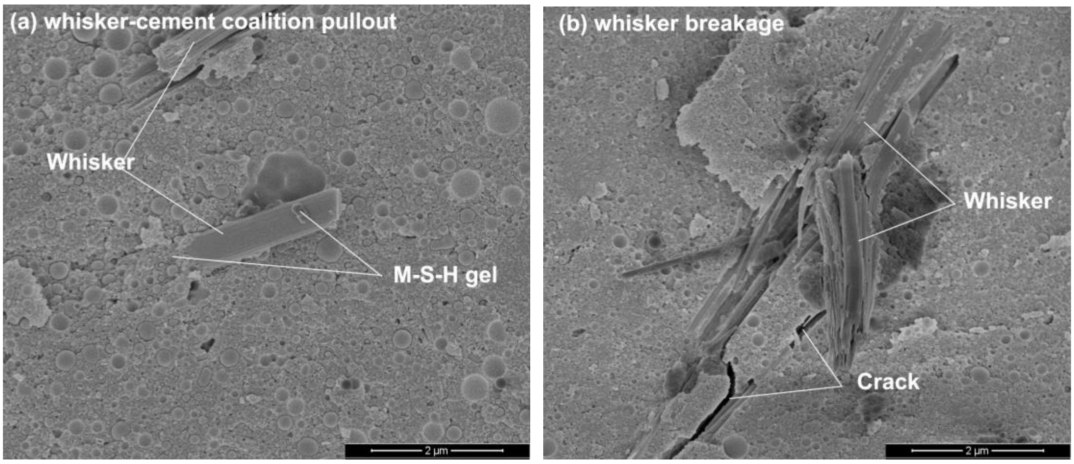

Fig.10. Reinforcement mechanisms of MHSH whiskers in the composites with 5 wt% whiskers.

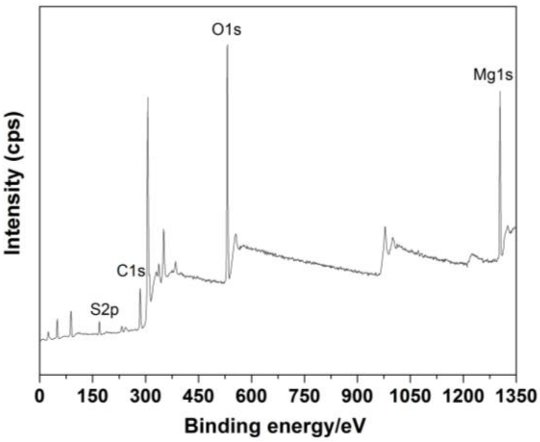

Fig.11. XPS spectra of MHSH whiskers.

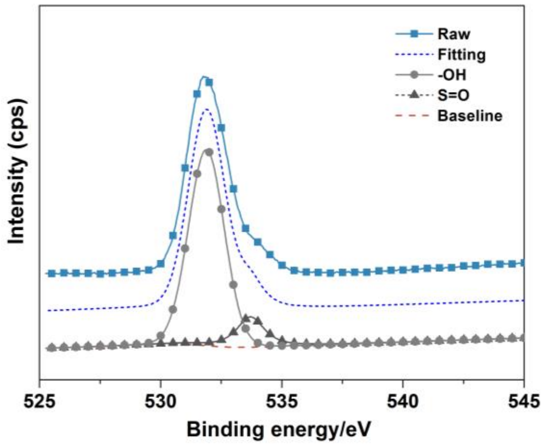

Fig.12. Curve-fitting of the O 1s spectra.

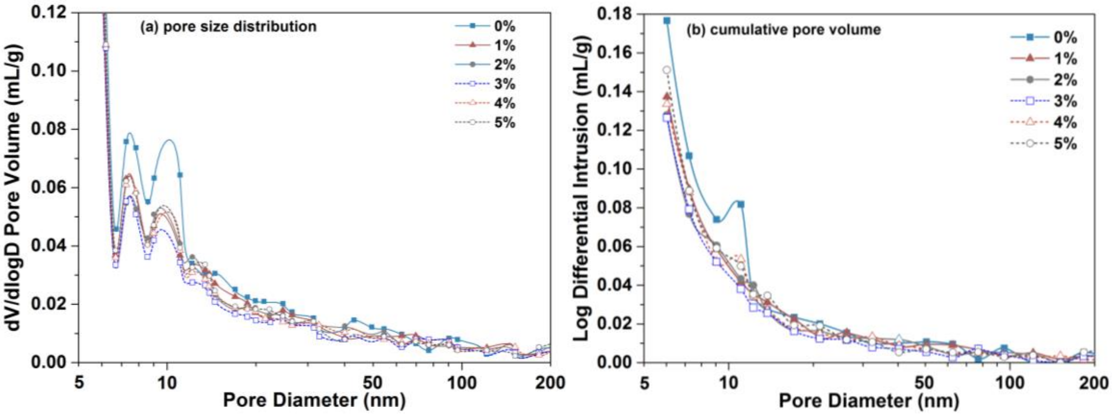

Fig.13. Differential curves of M-S-H cement with 0 - 5 wt% MHSH whiskers.

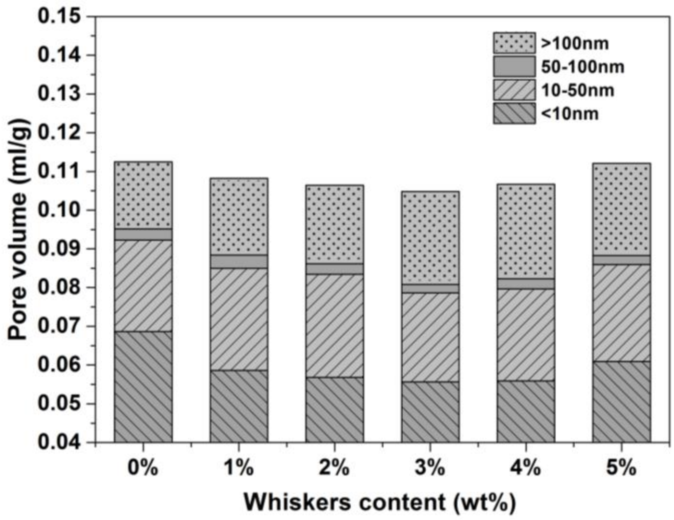

Fig.14. Porosity and pore volume distribution of M-S-H cement with 0 - 5 wt% MHSH whiskers.

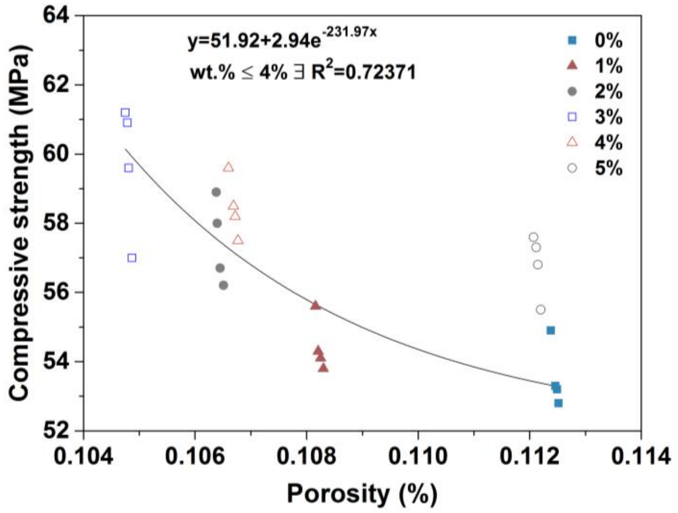

Fig.15 Equations between compressive strength and porosity of M-S-H based on Ryshkevitch equation.

Table 1

Chemical compositions of the raw materials.

wt%	MgO	SF	MHSH
SiO_2	0.35	94.71	0.07
Al_2O_3	0.07	0.23	0.05
Fe_2O_3	0.15	0.24	--
CaO	0.87	0.68	--
P_2O_5	--	0.37	--
MgO	98.3	1.19	70.18
K_2O	--	1.74	--
Na_2O	--	0.35	--
SO_3	0.05	0.36	29.68
Cl	--	0.09	--

Table 2

Ratio of raw materials for the preparation of M-S-H cement mortars.

Whiskers (wt%)	MgO g	SF g	Sand g	Water g	Na-HMP g	Whiskers g
0	240	360	600	330	12	0
1	240	360	600	330	12	6
2	240	360	600	330	12	12
3	240	360	600	330	12	18
4	240	360	600	330	12	24
5	240	360	600	330	12	30

Table 3

Flexural load-deflection data of M-S-H mortars with different MHSH whisker contents.

Whiskers (%)	0	1	2	3	4	5
Load (kN)	2.187	2.267	2.337	2.455	2.626	2.409
Deflection (mm)	1.408	1.209	1.333	1.057	1.601	1.870